Applied Surface Science 257 (2011) 9299–9305

Contents lists available at ScienceDirect

Applied Surface Science

journal homepage: www.elsevier.com/locate/apsusc

Effects of thermal treatment on femtosecond laser fabricated diffraction gratings in polystyrene

K.L.N. Deepak[a], S. Venugopal Rao[b], D. Narayana Rao[a,*]

[a] School of Physics, University of Hyderabad, Hyderabad 500046, India
[b] Advanced Center of Research in High Energy Materials, University of Hyderabad, Hyderabad 500046, India

ARTICLE INFO

Article history:
Received 14 April 2011
Received in revised form 4 May 2011
Accepted 4 May 2011
Available online 12 July 2011

Keywords:
Diffraction Gratings
Femtosecond laser writing
Emission spectrum
Excitation spectrum
Raman spectrum
Optical centers

ABSTRACT

We report the fabrication of efficient, buried diffraction gratings and micro-craters in bulk polystyrene using femtosecond laser direct writing technique. We recorded a maximum diffraction efficiency of 10% for a buried grating fabricated at 1 μJ energy, 1 mm/s speed, and a period of 30 μm. Buried micro-craters, with typical dimensions of ~2 μm, were achieved at low energies and high scanning speeds. From the field emission scanning electron microscope studies, the observed emission is attributed as due to the inner surface modifications and the debris settled around the voids. The fabricated gratings subjected to heat treatment were tested for the diffraction efficiency and emission at different excitation wavelengths and the observed results are presented. Raman spectra collected from the femtosecond laser modified regions revealed the disappearance of few Raman modes at high peak intensities associated with incident Gaussian laser pulse. Potential applications of these luminescent micro-craters are highlighted.

1. Introduction

When femtosecond (fs) pulses are focused within the volume of a dielectric material, nonlinear excitation can lead to physical processes such as avalanche ionization, electron plasma formation and shock-wave induced micro-explosions. Compared with continuous wave and long-pulsed lasers, fs laser pulses have two apparent features: (1) thermal effect elimination due to extremely short energy deposition time and (2) participation of various nonlinear processes enabled by high localization of laser photons in both time and spatial domains. Due to these factors material processing with fs laser is generally characterized by the absence of heat diffusion and molten layers [1]. Moreover, the nature of ultrashort light–matter interaction permits fs laser to overcome the diffraction limit [2]. Mourou and co-workers have carried out pioneering investigations on the mechanisms and applications of the femtosecond laser processing, especially on the material surface [2–10]. A range of applications have resulted from these structures which include three-dimensional optical data storage [11,12], fabrication of optical waveguides [13–18], micro-structuring of optical components [16–18] and fabrication of micro-channels [19,20], photonic band gap structures [21,22], and Bragg gratings [23,24] in a variety of materials such as glasses and polymers. Polymers substrates possess many advantages over their glass counterparts since they are cost-effective and their properties can easily be tailored for specific applications. One of the advantages of polymers for micro-structuring is their lower threshold for optical breakdown, which can be achieved using non-amplified nanoJoule femtosecond pulses. Considerable research has been carried out on the microstructures fabricated in polymers. We had earlier successfully fabricated surface and buried gratings in thin films and bulk of poly methyl methacrylate (PMMA) and poly dimethyl siloxane (PDMS) using fs pulses [25] and characterized the structures using laser confocal and scanning electron microscopy (SEM) techniques. We also observed emission from the fs fabricated structures in PMMA, PDMS, poly vinyl alcohol (PVA) and polystyrene (PS) and identified the mechanisms responsible for emission using the techniques of ESR, excitation and emission spectroscopy, and Raman spectroscopy [26–28]. Herein we present some of our results on the fabrication of buried gratings in PS and the effects of thermal treatment on their emission properties. We have also achieved micro-craters on the surface of PS and the optical properties of these structures were examined using micro-Raman spectroscopy.

2. Experimental

Full details of the experimental set up have been reported in our earlier publications [25–32]. In brief, the laser source used was a Ti:sapphire oscillator–amplifier system operating at a wavelength of 800 nm delivering ~100 fs pulses, ~1 mJ output energy pulses

* Corresponding author. Tel.: +91 040 23134335.
E-mail addresses: dnrsp@uohyd.ernet.in, dnr.laserlab@gmail.com (D.N. Rao).

0169-4332/$ – see front matter © 2011 Elsevier B.V. All rights reserved.
doi:10.1016/j.apsusc.2011.05.019

Table 1
Details of micro fabrication of gratings in PS.

S. No.	Terminology	Energy (μJ)	Speed (mm/s)	Period (μm)	Width (μm)	Type of structure
1	PSG1	1	0.5	30	16	Line
2	PSG2	0.635	0.5	30	21	Line
3	PSG3	0.033	0.5	30	3	Line
4	PSG4	0.033	3	30	2	Crater
5	PSG5	1	3	30	4	Line
6	PSG6	1	2	50	11	Line
7	PSG7	1	0.5	100	20	Line
8	PSG8	1	2	30	5	Line
9	PSG9	1	1	30	12	Line
10	PSG10	1	1	20	11	Line
11	PSG11	1	1	50	12	Line

with a repetition rate of 1 kHz. The near-transform limited nature of pulses was confirmed from the time-bandwidth product. Three translational stages (Newport) were arranged three dimensionally to translate the sample in all *x*, *y*, and *z* directions. Laser energy was varied using the combination of half wave plate and a polarizer. We have used 40× (Numerical Aperture (NA) of 0.65) microscope objective in our experiments for focusing. We fabricated buried diffraction gratings in bulk polystyrene purchased from Goodfellow, UK. These polymers were cut into 1 cm × 1 cm square area for our experiments. Edges were polished and sonicated for 1 h in distilled water to remove the dust and unwanted debris before fabrication experiment is carried out.

3. Results and discussion

Several buried diffraction gratings were fabricated in the bulk of PS using fs pulses at different scanning speeds, energies and periods. Details of various parameters used in the fabrication of these gratings are tabulated in Table 1. Each grating with its particular set of writing parameters is given a code for simplicity. Fig. 1(a) shows the confocal microscope image of PSG1 grating and its diffraction pattern captured by a CCD camera (shown in the middle of the figure). The structure was fabricated at 1 μJ energy, 0.5 mm/s speed with 30 μm period. We found some interesting effects in our microfabrication experiments while working with reduced energy and

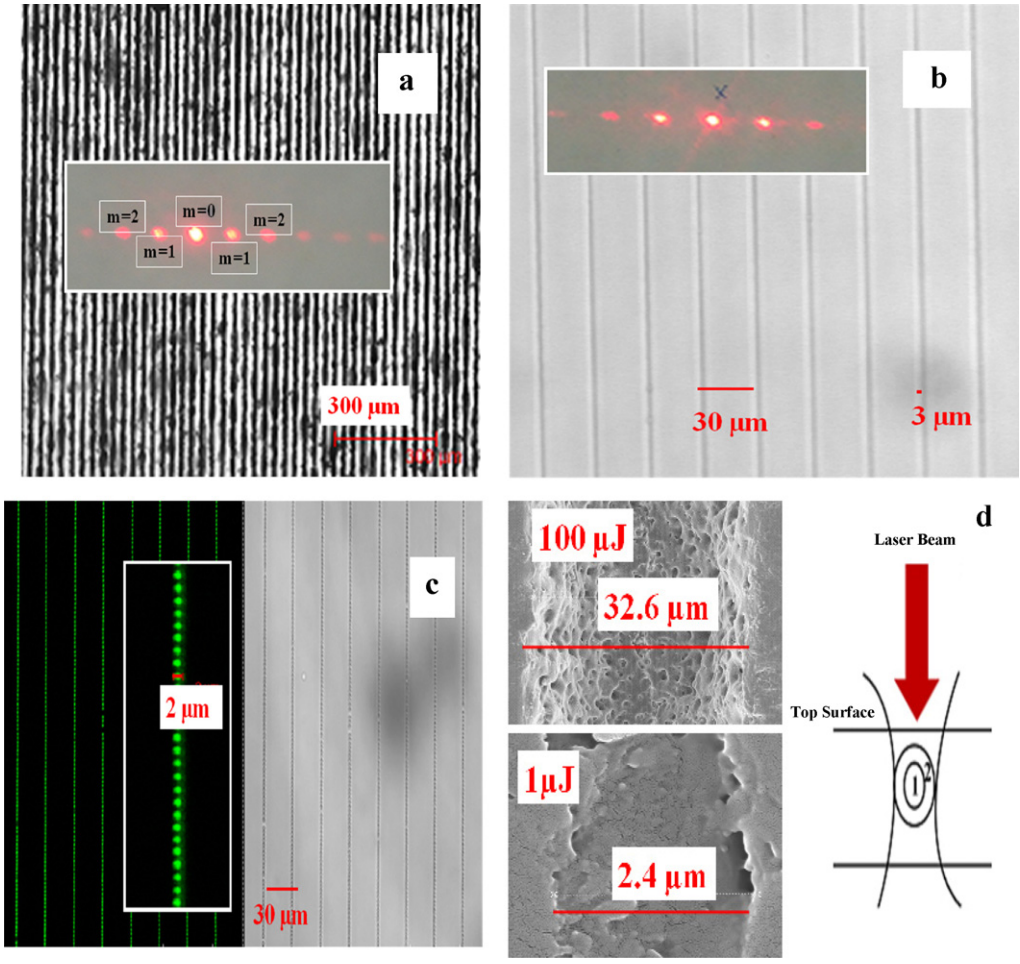

Fig. 1. Confocal microscope image of a typical buried PSG1 grating,Inset shows diffraction pattern with different orders, Scale bar is 300 μm. (b) Confocal microscope image of PSG3 grating and the corresponding diffraction pattern (period 30 μm and width 3 μm). (c) Confocal microscope image of PSG4 grating (period 30 μm). Pseudo green color indicates emission from the fs laser modified regions when excited at 488 nm wavelength, Array of luminescent micro-craters is depicted in middle with crater size of ~2 μm. (d) FESEM images of surface structure fabricated at 100 and 1 μJ energy with 1 mm/s speed. Right side picture shows a schematic diagram showing the two regions from where the fluorescence was collected. (For interpretation of the references to color in this figure legend, the reader is referred to the web version of the article).

Table 2
Details of micro crater structures fabricated at different energies and scanning speeds.

S. No.	Energy (nJ)	Speed (mm/s)	Observation (Line/Crater)	Structure/Crater size (μm)
1	1000	1	Line	12
		1.5	Line	10
		2	Line	10
		2.5	Crater formation started	6
		3	Crater	6
		3.5	Crater	4
		4	Crater	3
		4.5	Crater	4
		5	Crater	3
2	635	1	Line	14
		1.5	Line	12
		2	Crater formation started	10
		2.5	Crater	3
		3	Crater	3
		3.5	Crater	3
		4	Crater	3
		4.5	Crater	3
		5	Crater	3
3	168	1	Line	4
		1.5	Crater formation started	3
		2	Crater	2
		2.5	Crater	2
		3	Crater	2
		3.5	Crater	2
		4	Crater	2
		4.5	Crater	2
		5	Crater	2
4	33	1	Line	3
		1.5	Crater formation started	3
		2	Crater	2
		2.5	Crater	2
		3	Crater	2
		3.5	Crater	2
		4	Crater	2
		4.5	Crater	2
		5	Crater	2

increased scanning speed. When the input energy was reduced typically from microJoule to nanoJoule, we obtained smooth structures and we believe the modification is of refractive index change. PSG3 grating is fabricated at 33 nJ energy and with 0.5 mm/s speed. Fig. 1(b) shows the confocal microscope image of the PSG3 grating and its diffraction pattern captured with a camera. When scanning speed is increased along with the reduced energy of the pulses we observed the formation of micro-craters instead of straight line structures. Fig. 1(c) shows the confocal microscope image of PSG4 fabricated at 33 nJ energy and 3 mm/s speed. We found micro-craters arrayed throughout the fabricated grating structure instead of straight lines. Left side of the figure shows pseudo-green color that represents the emission when excited at 488 nm wavelength. For clarity, one array of craters is shown in the inset of Fig. 1(c). By decreasing the energy a weaker source for thermal diffusion is generated resulted in reduced modified size and by increasing the scan speed there was a reduction of pulse to pulse overlap [33]. Thus, one can achieve micro-craters instead of straight line structures at low energies and high scanning speeds. The material that is ablated from the center of the higher energy Gaussian pulse gets deposited on the inner surface of the voids. The debris shows emission which can be seen when excited with 488 nm wavelength in the confocal geometry. Therefore top, bottom and sides of the irradiated region show emission. Fig. 1(d) shows field emission scanning electron microscope (FESEM) images of two surface structures fabricated in PS at 100 and 1 μJ energy with 1 mm/s speed. Clearly we observed a trough and debris settled at the ends. The debris settled on the inner surfaces of the void along with the laser irradiated regions

Table 3
Diffraction efficiencies of buried PS gratings before and after thermal treatment.

S. No.	Grating type	Before thermal treatment (Percentage of DE)				After thermal treatment (Percentage of DE)			
		0th order	1st order	2nd order	3rd order	0th order	1st order	2nd order	3rd order
1	PSG1	27.1	8.3	0.65		14	4.96	0.4	
2	PSG2	21.2	7.95	0.40		46	6.87	1.7	0.26
3	PSG3	93	0.26	0.49		82	0.43	0.4	0.32
4	PSG4	96	0.19	0.17		90	0.43	0.18	
5	PSG5	85	0.13	0.74		96	0.328	0.3	
6	PSG6	66	3.65	1.5		72	2.21	1.6	0.89
7	PSG7	48	6.63	3.11	0.58	64	4.28	2.61	
8	PSG8	88	3.68	0.86	0.4	86	1.13	0.74	
9	PSG9	30	10	1.3		31	7.2	0.68	
10	PSG10	20	6.8	0.25		7	3	0.47	
11	PSG11	65	1.79	1.07	1	43	2.27	1.44	

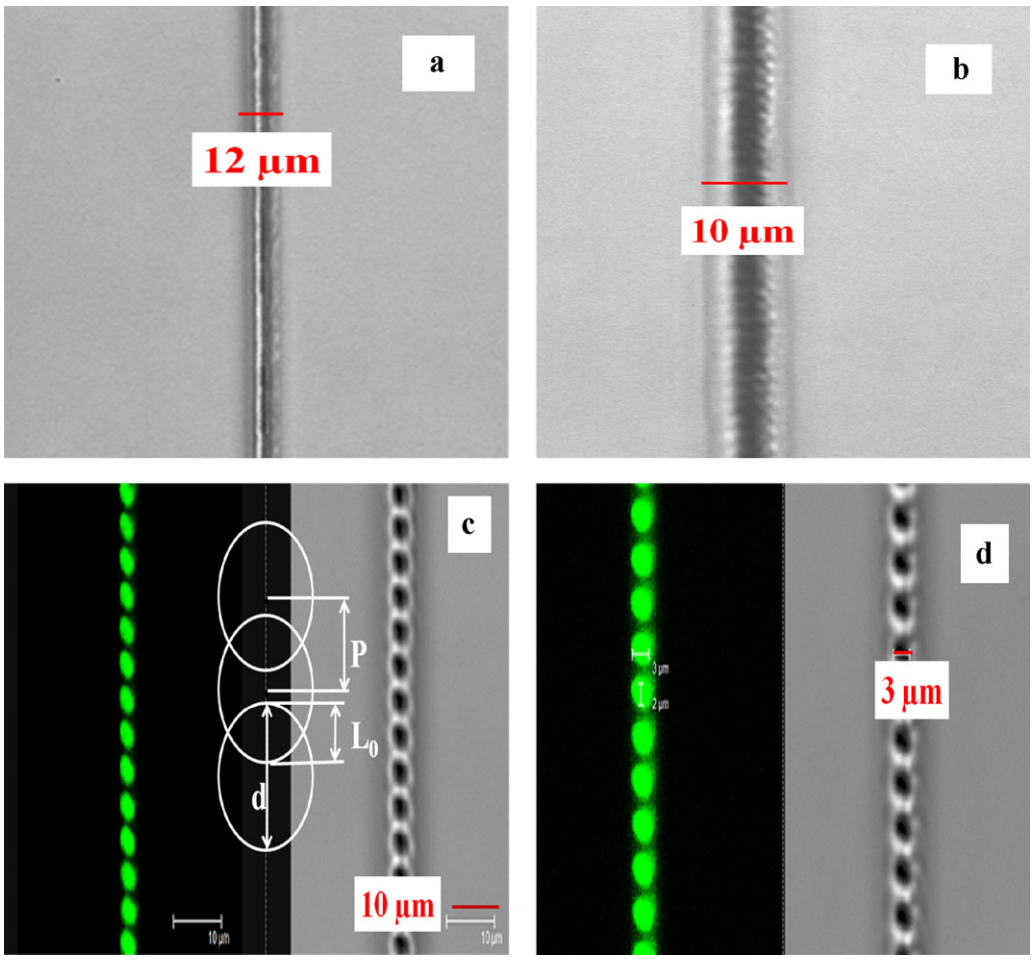

Fig. 2. (a) Confocal microscope images of a buried single micro-structure in PS fabricated at 1 μJ energy and 1 mm/s speed. Structure width is ~12 μm. (b) Beginning of formation of micro-craters at the same energy when scanning speed is increased to 2 mm/s. Structure width 10 μm. (c) Scanning speed increased to 3 mm/s and the inset shows model used to fabricate micro-craters. (d) Confocal microscope image of the craters formed at still higher scanning speed that is a mm/s. Pseudo green color indicates emission from the modified micro-craters when excited at 488 nm wavelength. Craters size is 3 μm. (For interpretation of the references to color in this figure legend, the reader is referred to the web version of the article).

contributes to the observed emission. Right side of Fig. 1(d) shows a schematic diagram with two regions of modification. Region 1 is completely of void type (due to middle portion of the incident Gaussian pulse) which is surrounded by region 2 of index change type which consists of ablated and modified material (tail portions of the incident Gaussian pulse).

We also fabricated structures at different energies (1 μJ, 635 nJ, 168 nJ, and 33 nJ) and different scanning speeds to study the formation of micro-craters in detail. The aspects of formation of craters (buried) at different energies and with different scanning speeds and size of craters obtained are tabulated in Table 2. Fig. 2(a) shows confocal microscope image of a buried single micro structure in PS fabricated at 1 μJ energy and 1 mm/s speed. For the same energy we observed the appearance of craters when the scanning speed was increased to 2 mm/s. This is depicted clearly in Fig. 2(b). The process of formation of micro-craters is evident from the edges of Fig. 2(b). Fig. 2(c) and (d) illustrate the confocal microscope images of the craters formed at still higher scanning speeds of 3 and 4 mm/s. From these data we confirmed that by increasing the scanning speed one can reduce the pulse to pulse overlap and the micro-craters can be obtained similar to observations of periodic refractive index modulation observed earlier in glasses [34]. The same trend was observed even at other energies also. However, we found that the formation of craters at higher scanning speeds and lower energies show better profiles. This is obvious because the intensity of heat waves generated at each position where the pulse impinges depends on the pulse energy. Hence, at higher energies these intense heat waves travel and overlap with the waves generated at other positions. This leads to the formation of a line instead of a crater. Inset of Fig. 2(c) shows a model that represents the formation of micro-craters. The pitch 'p' which is the distance from center to center can be varied by setting the scanning speed according to the relation $p = s/f$ where 's' is scanning speed and 'f' is laser repetition frequency which is 1 kHz in our case. L_0 is the overlap region between two consecutive focused spots which is $(d - p)$ where d is the diameter of the spot. The spot size is calculated using the relation $D = 1.22\ \lambda/\mathrm{NA}$ where D is the diameter of the focused spot, λ is the wavelength and NA is the numerical aperture of the microscope objective used [25,29,35]. We had used a 40× microscope objective with NA of 0.65 in our experiments. The estimated spot size was 1.55 μm. In our experiments on micro-crater fabrication we observed clear micro-crater formation from 3 mm/s speed onward with different energies as tabulated in Table 2. Hence the minimum pitch (p) can be taken as 3 μm. As the radius of the focused spot is ~0.75 μm, the micro craters start appearing for speeds beyond 3 mm/s. However, we could obtain minimum crater size of ~2 μm in our experiments owing to the size of the focused spot and continuous translation. The fabrication of these micro craters is useful in the areas of memory storage devices and photonic crystals [25–28,36–38].

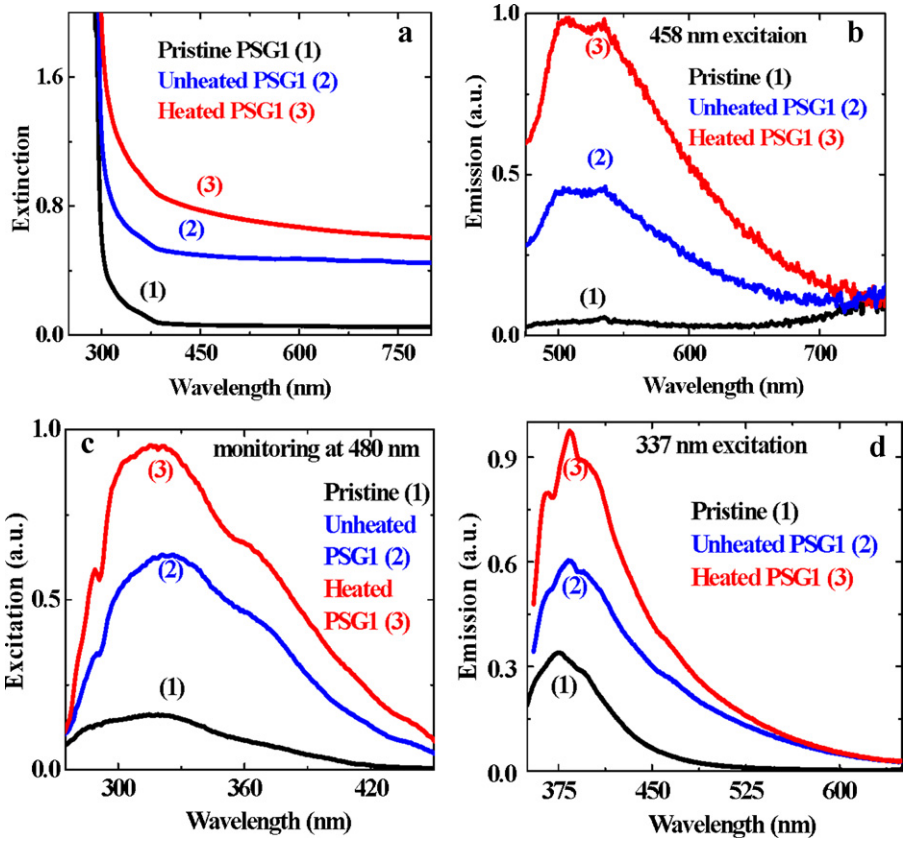

Fig. 3. (a) The extinction spectra that include absorption, scattering and diffraction losses for pristen PS, fs laser irradiated, and thermally treated + fs laser irradiate PSG1. (b) Emission spectra obtained for pristen PS, fs laser irradiated, and thermally treated + fs laser irradiated PSG1 when excited at 458 nm wavelength. (c) Excitation spectra obtained for pristen PS, fs laser irradiated, and thermally + fs laser irradiated PSG1 monitoring emission at 480 nm. (d) Emission spectra obtained for pristen PS, fs laser irradiated, and thermally treated + fs laser irradiated PSG1 when excited at 337 nm wavelength.

We used a He–Ne laser (633 nm) and measured the diffraction efficiencies of different gratings fabricated. Diffraction efficiency (DE) of *m*th order is calculated as the ratio of the power transmitted in the *m*th order to the incident power. Hirono et al. [39] reported an increment in the DE of gratings in PMMA obtained with 120 fs pulses through heat treatment at 70 °C for 500 h. The efficiency recorded was 1.9% before heat treatment and increases to 72% after heat treatment. They attributed the increase due to the increase in induced RI change after heating and suggested the physical mechanism responsible was volume contraction at the irradiated region.

Table 3 shows the DE results obtained with these gratings. Since most of these gratings were fabricated at higher energies, the modification in the fs laser irradiated regions would be of void type. Therefore, we did not observe any appreciable increment in the DE with thermal treatment. However we did observe a clear enhancement in the emission and absorption properties of the irradiated regions. We recorded emission and excitation spectra using a fluorescence spectrometer. There are a few reports on luminescent properties of glasses after they are treated with fs laser [40,41]. We showed similar results on emission and paramagnetic behavior of these polymers irradiated with fs laser [25–29]. The emission observed in fs laser irradiated regions is mainly attributed to the generation of optical centers such as *trans*-stilbene, diphenylbutadiene (DPBD), and diphenylhexatriene (DPHT) [26–28]. Fig. 3(a) shows the extinction spectra obtained for pristine PS, irradiated PS (PSG1) and irradiated PS (PSG1) after thermal treatment. We found that the losses of the irradiated PSG1 increase in comparison to the pristine PSG1 due to the formation of optical centers or luminescent centers. Heat treated fs laser irradiated PSG1 showed further increase in the losses due to further formation of optical centers upon thermal treatment which could be due to bond breakage. The optical centers formed showed emission when excited at 458, 488, and 514 nm wavelengths. The losses that we observed in Fig. 3(a) are due to absorption from optical centers, scattering and diffraction. In order to estimate the losses due to scattering and diffraction, we have recorded the absorption spectrum with a fiber spectrometer, with the fiber tip kept immediately after the irradiated portion of the sample. We observed that transmittance comes down by only 41% in comparison to the transmittance coming down by 60% while recording with the UV–vis spectrometer. This indicates that the loss due to scattering and diffraction is nearly 19%. Therefore, depending on the type of application, one can control the formation of optical centers by irradiation at higher fluences or pure index grating at low fluences leading to diffraction. Formation of optical centers would be more suited for memory devices, while pure index grating with lower absorption losses is ideal for the diffraction applications. Fig. 3(b) shows the emission of pristine PS and PSG1 grating before and after heat treatment when excited at 458 nm. There was no emission observed from pristine PS. PSG1 grating demonstrated emission when excited at 458 nm due to formation of optical centers [27,28]. Because of the increased absorption from the optical centers, emission too shows an increase upon heating. We reported earlier that the emission intensity increases with the irradiation energy, which is due to the formation of more optical centers [25,28]. Fig. 3(c) shows excitation spectra collected by monitoring the 480 nm emission wavelength. Excitation spectra at different monitoring wavelengths showed maximum absorption or excitation at 337 nm. Fig. 3(d) shows the emission spectra with 337 nm as the excitation wavelength. This emission is attributed to the optical centers of *trans*-stilbene (364 nm) and DPBD (383 nm).

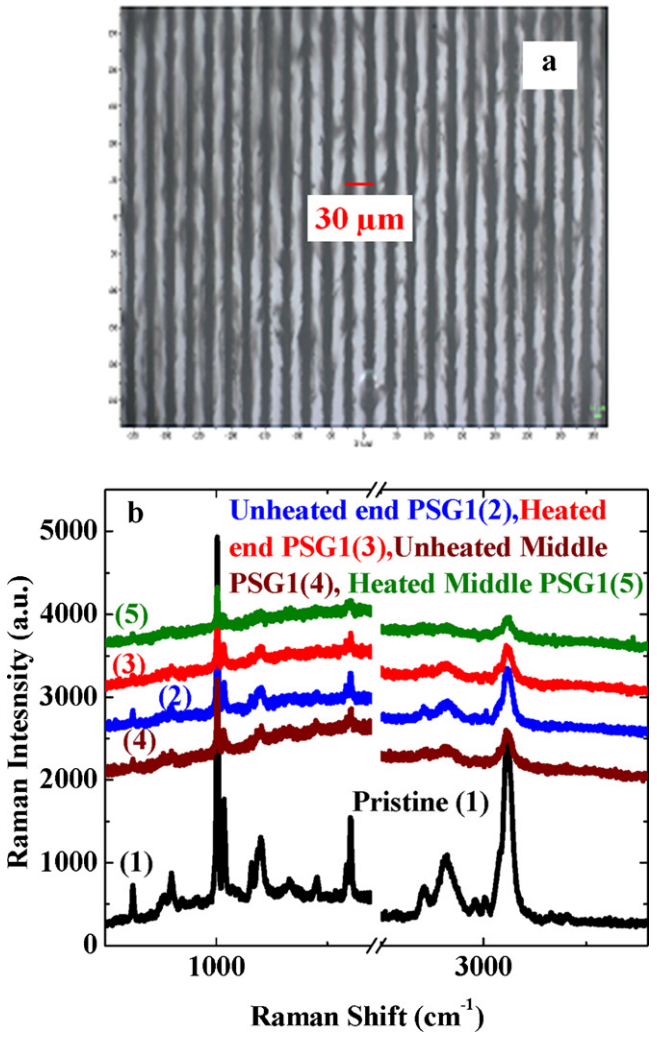

Fig. 4. (a) Microscope image of PSG1 grating, scale bar and period is 30 μm. (b) Raman plot of pristen PS, irradiated PSG1, heated and irradiated PSG1 with central and end regions of the modifications.

Table 4
Raman mode assignments for PS.

S. No.	Raman shift (cm^{-1})	Assignment
1	398	No reference found
2	624	Ring mode (υ_{6b}) which supports either mono or para substitution
3	761	Out of plane CH bend for mono or para substitution
4	800	Finger print band of styrene
5	1004	Ring breathing mode
6	1032	Styrene group
7	1158	bands
8	1201	
9	1332	No reference found
10	1454	CH_2 or CH_3 bending modes
11	1587	υ_{8a} and υ_{8b} aromatic ring stretch
12	1604	(Aromatic ring deformation)
13	2853	sp^3 CH group
14	2907	
15	2980	
16	3004	sp^2 CH group
17	3056	

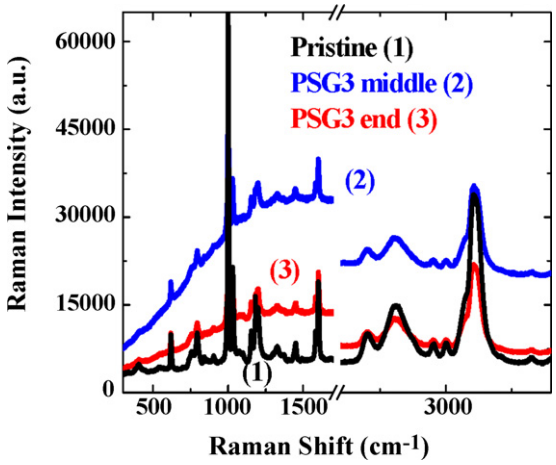

Fig. 5. Raman plots of pristine PS (1), fs irradiated PSG3 central region (2) and end region (3).

We observed similar trends in the emission spectra at different excitation wavelengths.

We recorded micro-Raman spectra in the confocal geometry for pristine PS and fs laser irradiated PSG1 without and with heat treatment. Table 4 enlists the Raman modes of PS [42,43]. Fig. 4(a) and (b) show the microscope image of PSG1 and Raman plots. Some of the Raman plots have been shifted (vertically) for clarity. We collected the Raman signal from the center and edge portions of the lines drawn in the PSG1 grating. The intensity of Raman modes are suppressed in case of fs laser irradiated PS. We observed that the intensities of two main Raman modes are affected drastically due to stress waves generated in the fs laser irradiated regions. 1001 and 1603 cm^{-1} modes of PS correspond to ring breathing and C=C vibrational modes respectively [42,43]. The two modes at 2980 and 3004 cm^{-1} corresponding to sp^3 and sp^2 CH groups disappeared completely in case of fs laser irradiated PS. Though we expect voids in the middle portion of the fabricated structures, there could be debris ablated and resettled in the middle portion of the structures which contribute to the Raman signal. Part of this signal could be from top and bottom portions of the line structures.

Raman spectrum of PSG3 grating fabricated at 33 nJ energy, 0.5 mm/s speed with 30 μm period is shown in Fig. 5. We observed that the Raman spectrum from the irradiated region is very similar to that of the pristine region. This is understandable as the phenomenon of bond breaking which leads to major structural changes does not take place at such low energies.

4. Conclusions

We presented our detailed experimental results on the fabrication and characterization of buried diffraction gratings and micro-craters in bulk PS using fs pulses. A maximum diffraction efficiency of 10% is recorded for a grating fabricated at 1 μJ energy, and 1 mm/s speed with 30 μm period. Through the FESEM and the Raman studies, we confirmed that the emission in the modified regions is due to optical centers created in the laser irradiated regions and the debris. Increase in emission and excitation intensities due to thermal treatment given to these gratings is presented. Raman analysis of different modes before and after irradiation indicated disappearance and intensity change for few modes at higher irradiation doses.

Acknowledgements

K. L. N. Deepak acknowledges the senior research fellowship from Council of Scientific and Industrial Research, India. D. Narayana Rao acknowledges financial support from the Department of Science and Technology, India. This research is performed

in the framework of ITPAR Phase II FaStFal 2007–2010 project. Financial support from the Research Center Imarat, Hyderabad, India is acknowledged.

References

[1] B.N. Chickov, C. Momma, S. Nolte, F.V. Alvensleben, A. Tunnermann, Appl. Phys. A 63 (1996) 109–115.
[2] P.P. Pronko, S.K. Dutta, J. Squier, J.V. Rudd, D. Du, G. Mourou, Opt. Commun. 114 (1995) 106–110.
[3] R. Suriano, A. Kuznetsov, S.M. Eaton, R. Kiyan, G. Cerullo, R. Osellame, Chichkov S B.N., M. Levi, S. Turri, Appl. Surf. Sci. 257 (2011) 6243–6250.
[4] P. Bizi-Bandoki, S. Benayoun, S. Valette, B. Beaugiraud, E. Audouard, Appl. Surf. Sci. 257 (2011) 5213–5218.
[5] L. He, J. Chen, D.F. Farson, J.J. Lannutti, S.I. Rokhlin, Appl. Surf. Sci. 257 (2011) 3547–3553.
[6] C.R. Mendonca, S. Orlando, G. Cosendey, M. Winkler, E. Mazur, Appl. Surf. Sci. 254 (2007) 1135–1139.
[7] W. Chang, M. Choi, J. Kim, S. Cho, K. Whang, Appl. Surf. Sci. 240 (2005) 296–304.
[8] A. Ovsianikov, A. Ostendorf, B.N. Chichkov, Appl. Surf. Sci. 253 (2007) 6599–6602.
[9] A.F. Lasagni, P. Shao, J.L. Hendricks, C.M. Shaw, D.C. Martin, S. Das, Appl. Surf. Sci. 256 (2010) 1708–1713.
[10] M.R. Cardoso, V. Tribuzi, D.T. Balogh, L. Misoguti, C.R. Mendonça, Appl. Surf. Sci. 257 (2011) 3281–3284.
[11] E.N. Glezer, M. Milosavljevic, L. Huang, R.J. Finlay, T.H. Her, J.P. Callan, E. Mazur, Opt. Lett. 21 (1996) 2023–2025.
[12] D. Day, M. Gu, Appl. Phys. Lett. 80 (2002) 2404–2406.
[13] K.M. Davis, K. Miura, N. Sugimoto, K. Hirao, Opt. Lett. 21 (1996) 1729–1731.
[14] D. Homoelle, S. Wielandy, A.L. Gaeta, N.F. Borrelli, C. Smith, Opt. Lett. 24 (1999) 1311–1313.
[15] A.M. Streltsov, N.F. Borrelli, Opt. Lett. 26 (2001) 42–43.
[16] M. Masuda, K. Sugiola, Y. Cheng, N. Aoki, M. Kawachi, K. Shihoyama, K. Toyoda, H. Helvajian, K. Midorikawa, Appl. Phys. A 76 (2003) 857–860.
[17] Y. Cheng, K. Sugioka, K. Midorikawa, M. Masuda, K. Toyoda, M. Kawachi, K. Shihoyama, Opt. Lett. 28 (2003) 1144–1146.
[18] Y. Cheng, K. Sugioka, K. Midorikawa, Opt. Lett. 29 (2004) 2007–2009.
[19] Y. Li, K. Itoh, W. Watanabe, K. Yamada, D. Kuroda, J. Nishii, Y. Jiang, Opt. Lett. 26 (2001) 1912–1914.
[20] M.S. Giridhar, K. Seong, A. Schulzgen, P. Khulbe, N. Peyghambarian, M. Mansuripur, Appl. Opt. 43 (2004) 4584–4589.
[21] G. Zhou, M.J. Ventura, M.R. Venner, M. Gu, Opt. Lett. 19 (2004) 2240–2242.
[22] M.J. Ventura, M. Straub, M. Gu, Appl. Phys. Lett. 82 (2003) 1649–1651.
[23] G.D. Marshall, M. Ams, M.J. Withford, Opt. Lett. 31 (2006) 2690–2691.
[24] H.B. Zhang, S.M. Eaton, J. Li, P.R. Herman, Opt. Lett. 31 (2006) 3495–3497.
[25] K.L.N. Deepak, D. Narayana Rao, S. Venugopal Rao, Appl. Opt. 49 (2010) 2475–2489.
[26] K.L.N. Deepak, R. Kuladeep, S. Venugopal Rao, D. Narayana Rao, Chem. Phys. Lett. 503 (2011) 57–60.
[27] K.L.N. Deepak, R. Kuladeep, D. Narayana Rao, Opt. Commun. 284 (2011) 3070–3073.
[28] K.L.N. Deepak, R. Kuladeep, V. Praveen Kumar, S. Venugopal Rao, D. Narayana Rao, Opt. Commun 284 (2011), 3074 (4pp).
[29] K.L.N. Deepak, S. Venugopal Rao, D. Narayana Rao, Pramana- J. Phys. 75 (2010) 1221–1232.
[30] K.C. Vishnubhatla, S. Venugopal Rao, R.S.S. Kumar, R. Osellame, S.N.B. Bhaktha, S. Turrell, A. Chiappini, A. Chiasera, M. Ferrari, M. Mattarelli, M. Montagna, R. Ramponi, G.C. Righini, D. Narayana Rao, J. Phys. D: Appl. Phys. 42 (2009) 205106 (7 pp.).
[31] K.C. Vishnubhatla, S. Venugopal Rao, R. Sai Santosh Kumar, S.N.B. Bhaktha, A. Chiappini, A. Chiasera, J. Laureyns, M. Ferrari, M. Mattarelli, M. Montagna, R. Osellame, R. Ramponi, G.C. Righini, S. Turrell, D. Narayana Rao, Proc. SPIE 6881 (2008) 688114 (10 pp.).
[32] K.C. Vishnubhatla, S. Venugopal Rao, R.S.S. Kumar, K. Shiva Prasad, P.S.R. Prasad, D. Narayana Rao, Proc. SPIE 6881 (2008) 688113 (11 pp.).
[33] S.M Eaton, H. Zhang, M.L. Ng, J. Li, W.-J. Chen, S. Ho, P.R. Herman, Opt. Express 16 (2008) 9443–9458.
[34] H. Zhang, S.M. Eaton, P.R. Herman, Opt. Express 14 (2006) 4826–4834.
[35] C. Wochnowski, Y. Cheng, K. Meteva, K. Sugioka, K. Midorikawa, S. Metev, J. Opt. A: Pure Appl. Opt. 7 (2005) 493–501.
[36] Z. Nie, H. Lee, H. Yoo, Y. Lee, Y. Kim, K.S. Lim, M. Lee, Appl. Phys. Lett. 94 (2009) 111912 (3pp).
[37] Z. Nie, K.S. Lim, H. Lee, M. Lee, T. Kabayashi, J. Lumin. 131 (2011) 266–270.
[38] Z.G. Nie, K.S. Lim, W.Y. Jang, H.Y. Lee, M.K. Lee, T. Kabayashi, J. Phys. D: Appl. Phys. 43 (2010) 485101 (6 pp.).
[39] S. Hirono, M. Kasuya, K. Matsuda, Y. Ozeki, K. Itoh, H. Mochizuki, W. Watanabe, Appl. Phys. Lett. 94 (2009) 241122 (3 pp.).
[40] M. Watanabe, S. Juodkazis, H.B. Sun, S. Matsuo, H. Misawa, Phys. Rev. B 60 (1999) 9959–9964.
[41] T. Kudrius, G. Slekys, S. Juodkazis, J. Phys. D: Appl. Phys. 43 (2010) 1–5.
[42] Y. Djaoued, S. Badilescu, S. Balaji, N. Seirafianpour, A.-R. Hajiaboli, R. Banan sadeghian, K. Braedley, R. Bruning, M. Kahrizi, V.-V. Truong, Appl. Spectrom. 61 (2007) 1202–1210.
[43] D.W. Mayo, F.A. Miller, R.W. Hannah, Course Notes on Interpretation of Infrared and Raman spectra, Wiley Interscience, 2003.